Naval Research Laboratory

Washington, DC 20375-5320

NRL/MR/5650--12-9376

Analysis of Photonic Phase-Shifting Technique Employing Amplitude-Controlled Fiber-Optic Delay Lines

MEREDITH N. DRAA
VINCENT J. URICK
KEITH J. WILLIAMS

Photonics Technology Branch
Optical Sciences Division

January 13, 2012

REPORT DOCUMENTATION PAGE

Form Approved
OMB No. 0704-0188

1. REPORT DATE *(DD-MM-YYYY)*	**2. REPORT TYPE**	**3. DATES COVERED** *(From - To)*
13-01-2012	Memorandum	01 January 2011 - 22 September 2011

4. TITLE AND SUBTITLE

Analysis of Photonic Phase-Shifting Technique Employing Amplitude-Controlled Fiber-Optic Delay Lines

5a. CONTRACT NUMBER

5b. GRANT NUMBER

5c. PROGRAM ELEMENT NUMBER

6. AUTHOR(S)

Meredith N. Draa, Vincent J. Urick, and Keith J. Williams

5d. PROJECT NUMBER

5e. TASK NUMBER
EW-271-003

5f. WORK UNIT NUMBER
6308

7. PERFORMING ORGANIZATION NAME(S) AND ADDRESS(ES)

Naval Research Laboratory, Code 5652
4555 Overlook Avenue, SW
Washington, DC 20375-5320

8. PERFORMING ORGANIZATION REPORT NUMBER

NRL/MR/5650--12-9376

9. SPONSORING / MONITORING AGENCY NAME(S) AND ADDRESS(ES)

Office of Naval Research
One Liberty Center
875 North Randolph Street, Suite 1425
Arlington, VA 22203-1995

10. SPONSOR / MONITOR'S ACRONYM(S)

ONR

11. SPONSOR / MONITOR'S REPORT NUMBER(S)

12. DISTRIBUTION / AVAILABILITY STATEMENT

Approved for public release; distribution is unlimited.

13. SUPPLEMENTARY NOTES

14. ABSTRACT

This report describes a fiber-optic link design for the long-haul remoting of HF antennas. The link presented here is intended for remoting the antenna element a distance upwards of 7.0 km (4.3 mi) but the theoretical treatment allows for the design and analysis of links for greater stand offs. The analysis is carried out using well-established theory and verified experimental data which are employed throughout. A complete list of supporting references is also provided. The fiber-optic link performance is summarized as a 7-km point-to-point link with a single radio-frequency input and output having the following performance metrics over the 2-30 MHz range: –0.86 dB gain, 21 dB noise figure, 116.7 dB-Hz$^{2/3}$ spurious-free dynamic range above 1-Hz bandwidth, and 0.14˚/˚C phase stability over temperature. These metrics are for the fiber-optic link only and throughout the report we compare this performance to various all-electric systems demonstrating that the fiber link is suitable for HF applications.

15. SUBJECT TERMS

Fiber optics
Analog photonics
HF photonics

16. SECURITY CLASSIFICATION OF:			**17. LIMITATION OF ABSTRACT**	**18. NUMBER OF PAGES**	**19a. NAME OF RESPONSIBLE PERSON**
a. REPORT	**b. ABSTRACT**	**c. THIS PAGE**			Vincent J. Urick
Unclassified	Unclassified	Unclassified	UU	29	**19b. TELEPHONE NUMBER** *(include area code)* (202) 767-9352

TABLE OF CONTENTS

EXECUTIVE SUMMARY

1. Concept and architecture for employing fiber-optic delay lines to achieve photonic phase-shifting is presented.
2. Theory for 1x3 coupler is presented and discussed. System is assembled and measurement is directly compared to theoretical calculations.
3. Conclusions are made based on results of measured 1x3 coupler system and theoretical analysis.
4. Appendices: Theory for 1x4 and the general 1xM coupler cases are discussed.

1. Introduction

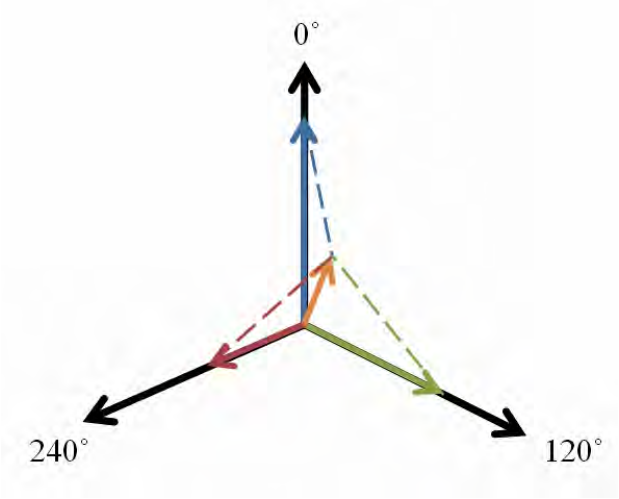

Figure 1: Phasor diagram showing three phase combination.

Optical phase shifting provides a numerous range of potential applications such as signal processing for RF systems and phase array antennas (PAA). For PAA applications, true time delay (TTD) is a well known solution for the beam squint problem [1]. One method of photonic phase shifting is achieved using the wavelength dependence of Brillouin frequency shift [2]. The development of wideband optical phased arrays and associated problems such as beam squint has been analyzed previously in [3, 4]. Architectures for fiber-optic TTD include noncompressive which is a brute force approach using optical switch or laser diode switches in parallel, delay-compressive which reduces the delay-dependent hardware complexity, and delay- and element-compressive which reduces the overall hardware using optical wavelength division multiplexing [4]. Phase shifters have been developed using heterodyne mixing [5, 6]. Recently, a system employing TTD was developed for 1-100GHz modulation range utilizing a fiber-coupled beam deflector and diffraction grating similar to a scanning delay line used for optical coherence tomography [7]. In this study we will investigate a novel method for employing phase shifting using an array of time delays and compare it to traditional TTD. Numerous fiber-based methods have been developed to obtain tunable TTD, however achieving optical phase shifting without changing fiber lengths can be useful for many applications. Looking at Figure 1, if we have three sinusoidal signals with 120˚ phase separation, by controlling the amplitudes we can achieve any phase angle desired with the appropriate combination. We will present a system that combines this simple methodology using a laser, Mach-Zehnder modulator, fiber-optic couplers, and fiber-optic delay lines to achieve RF phase shift.

Manuscript approved October 11, 2011.

2. Architecture

Figure 2 shows the general architecture for a system for phase shifting employing amplitude-controlled fiber-optic delay lines. A RF signal is modulated onto the optical amplitude of laser light with a Mach Zehnder modulator (MZM). Following the MZM is a 1×M coupler. The output ports are followed with a length of fiber to induce a time delay (τ) that is tuned to correspond to a desired phase for a specific frequency. The fiber is followed by a variable optical attenuator which will be used to control the input amplitude to the receiving photodiode. Finally, the photocurrent from each photodiode will be added together. For initial mathematical discussions we will look at the general case of adding a sine wave with the appropriate time delay as a phase shift with an amplitude that can be varied.

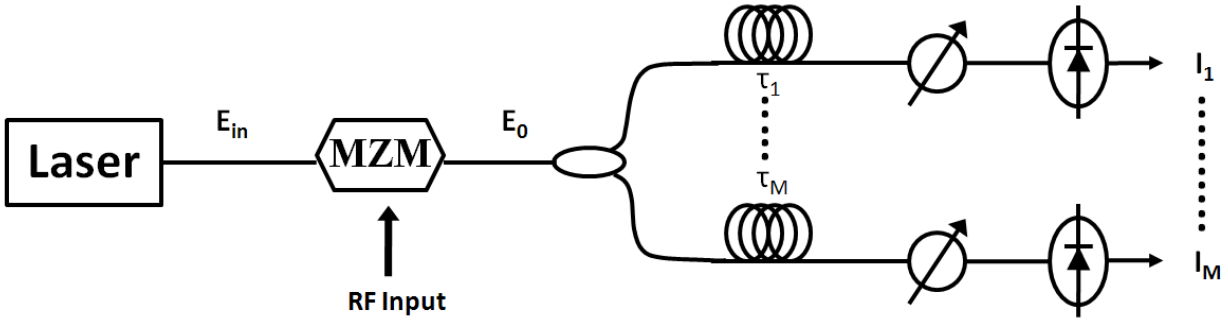

Figure 2: A laser is externally modulated by a MZM which is output to a 1×M coupler. At each output of the coupler is a delay line that corresponds to a phase shift as a designated frequency. A VOA precedes the detector. The photocurrents resultant will be added together.

3. Theory for 1x3 Coupler (M=3)

Starting with the case that corresponds to a 1×3 coupler which will have phase shifts corresponding to 0 and 120 and 240 degrees the photocurrent for each receiver will be:

$$I_n = A_n \sin(2\pi f(t + \tau_n)) \quad (1)$$

where $\tau_1 = 0$, $\tau_2 = 1/6f_0$ and $\tau_3 = 1/3f_0$where f_0 is the frequency that the time delay is centered on. The current is then added together to get the total at the output:

$$I_T = A_1 \sin(2\pi f t) + A_2 \sin(2\pi f(t + 1/6f_0)) + A_3 \sin(2\pi f(t + 1/3f_0)) \quad (2)$$

Equation (2) is plotted in Figure 3 as renormalized photocurrent vs. time for $f_0 = 20GHz$ and $f = 20GHz$ with the amplitudes varied from 0 to 1 with 0.5 step size. From the graph, it is obvious a large amount of phase shift occurs at 20GHz.

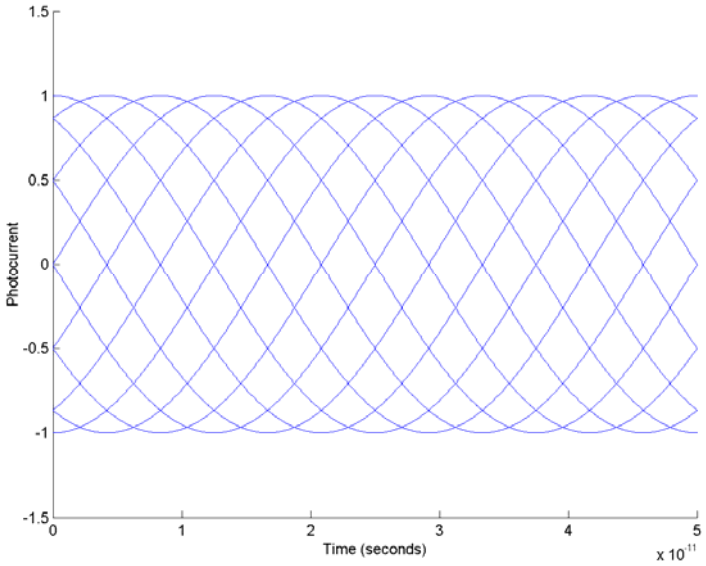

Figure 3: Renormalized photocurrent vs. time for at 20GHz with amplitudes varied from 0 to 1.

The phase vs. frequency is plotted in Figure 4 with amplitudes varied from 0 to 1 with 0.5 step size. There are frequencies at which there is only 0 or 180 degrees phase shift, which correspond to $f = (3k - 1.5)f_0$ where k=1, 2, 3,… Additionally, the phase shift corresponds to multiples of 360 degrees when $f = (3k)f_0$. To get a better view of the phase shift, Figure 5 is a zoomed in view of Figure 4 from 0 to 20GHz, where the red highlights an example of the shape of the phase shift curve as a function of frequency.

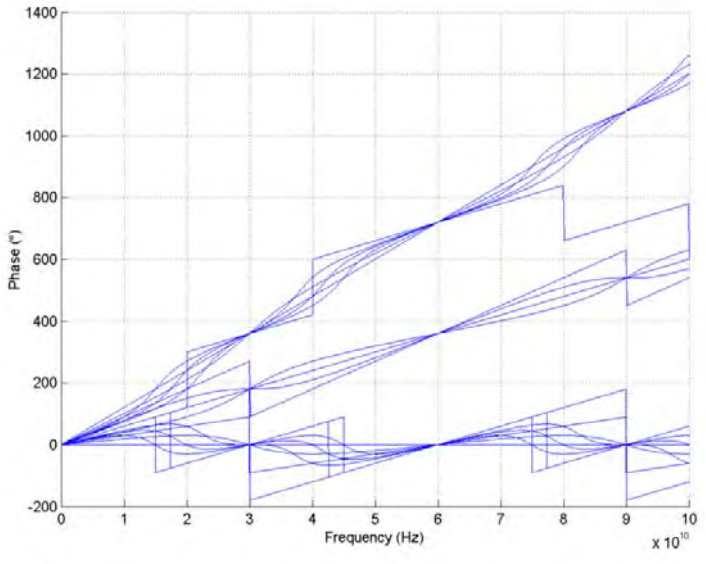

Figure 4: Phase vs. frequency for 1×3 coupler with amplitudes varied from 0 to 1 in 0.5 steps.

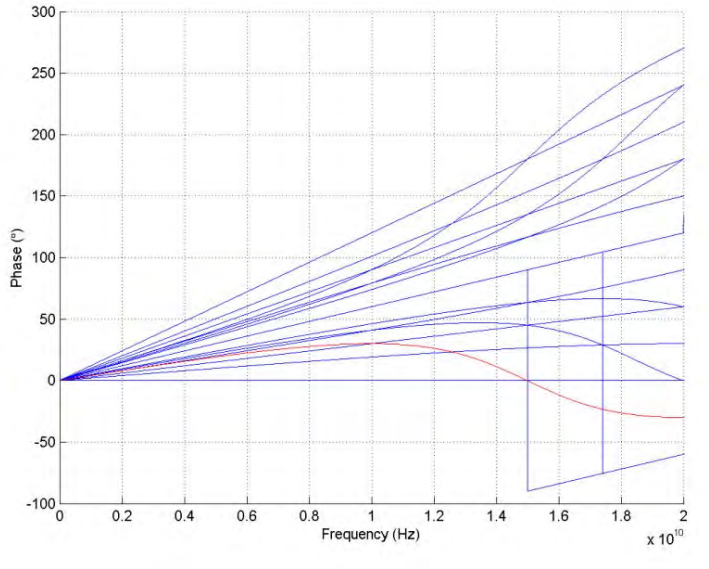

Figure 5: Zoomed in view of Figure 6 from 0-20GHz.

Next phase and amplitude are plotted as a function of frequency for a specific set of coefficients in Figure 6, demonstrating strong residual amplitude change with phase shift. Using (1) for the 1x3 coupler with coefficients A_1=0.23, A_2=0.45, A_3=0.87 at 20GHz center frequency, it is clear the inflection points for the phase occur at every 15GHz. The amplitude has a major peak at 0 and 60GHz, which is where the phase has an inflection point at 0 degrees, and minor null at 30GHz, which is where the phase has an inflection point at 180 degrees. The major nulls in the amplitude occur at a point of inflection of the derivative of the phase which is plotted in Figure 7 along with amplitude to illustrate this.

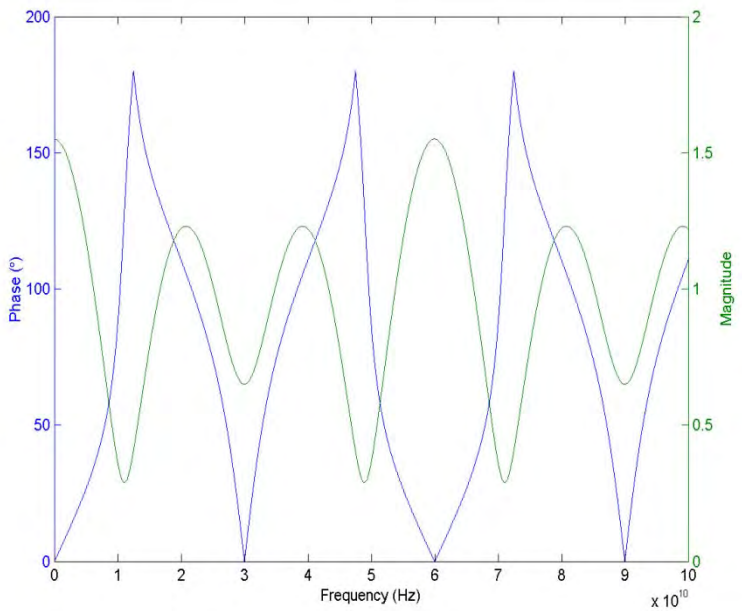

Figure 6: Phase (blue) and amplitude (green) vs. frequency for coefficients A_1=0.23, A_2=0.45, A_3=0.87.

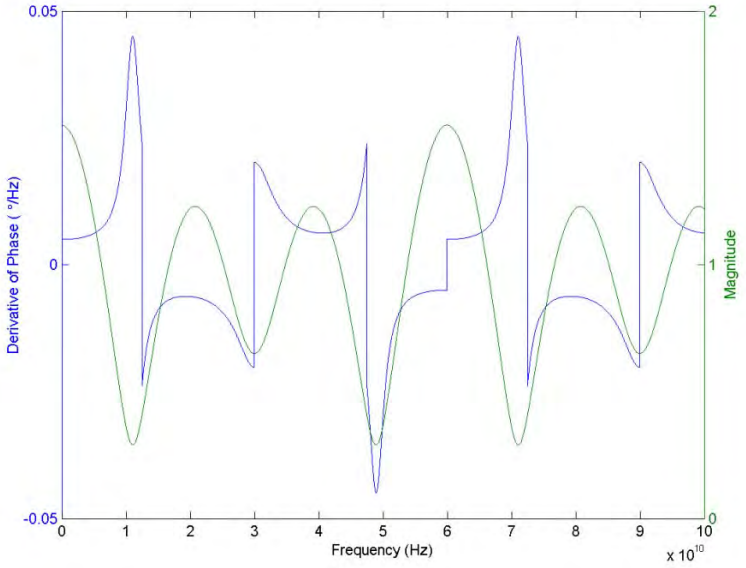

Figure 7: Derivative of phase (blue) and amplitude (green) vs. frequency for coefficients A_1=0.23, A_2=0.45, and A_3=0.87.

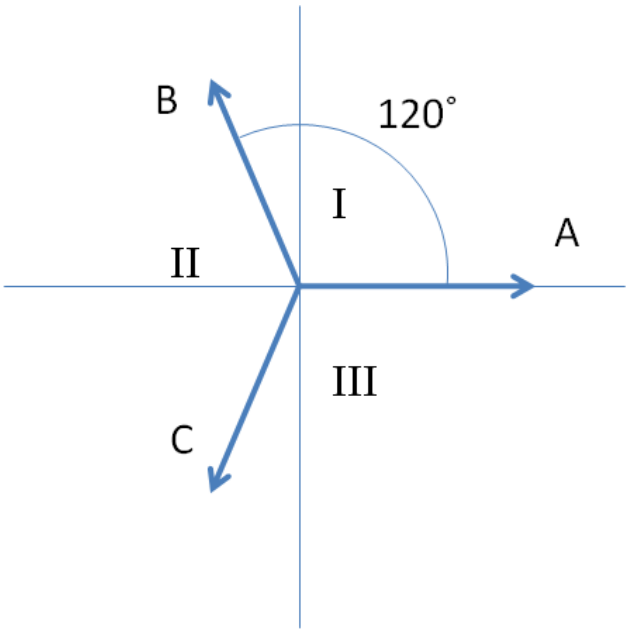

Figure 8: Diagram of each vector used to solve for constant amplitude for 1x3 coupler.

To make the system more useful we'd like to have 360˚ phase control with constant amplitude. The three vectors are plotted in Figure 8 where we'd like to be able to control the system so that the amplitude is a circle with radius $\sqrt{3}/2$ on the coordinate system. The general equations for the circle are:

$$\sqrt{3}/2 = \sqrt{(A - B/2 - C/2)^2 + \left(\frac{\sqrt{3}}{2}B - \frac{\sqrt{3}}{2}C\right)^2} \tag{3}$$

$$\theta = tan^{-1}\left(\frac{\frac{\sqrt{3}}{2}B - \frac{\sqrt{3}}{2}C}{A - B/2 - C/2}\right) \tag{4}$$

With two equations and three unknowns, we solve the equations in three parts. Instead of quadrants we can use the three 120˚ sections between the vectors (labeled in roman numerals in Figure 8) by setting one vector equal to zero for each solution, so that we have only 2 equations and 2 unknowns. The equations are solved in Mathematica and input into Matlab to graph the results based on the generated coefficients. The equations were solved with 1˚ precision for θ, so that there are 360 solutions. The results are plotted in Figure 9 as a function of the index which will be more or less values depending on the precision of phase solved for.

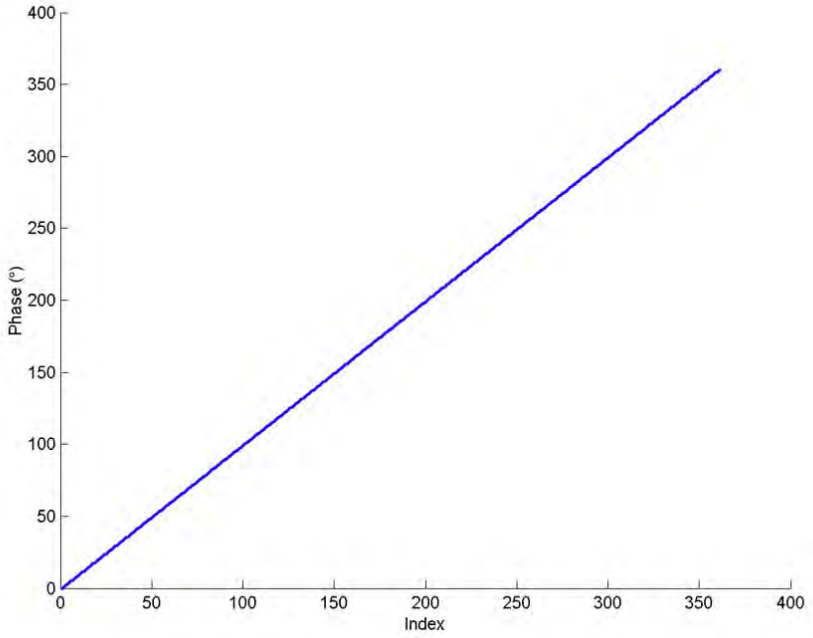

Figure 9: Phase as a function of index for 20GHz for 1x3 coupler with constant amplitude $\sqrt{3}/2$.

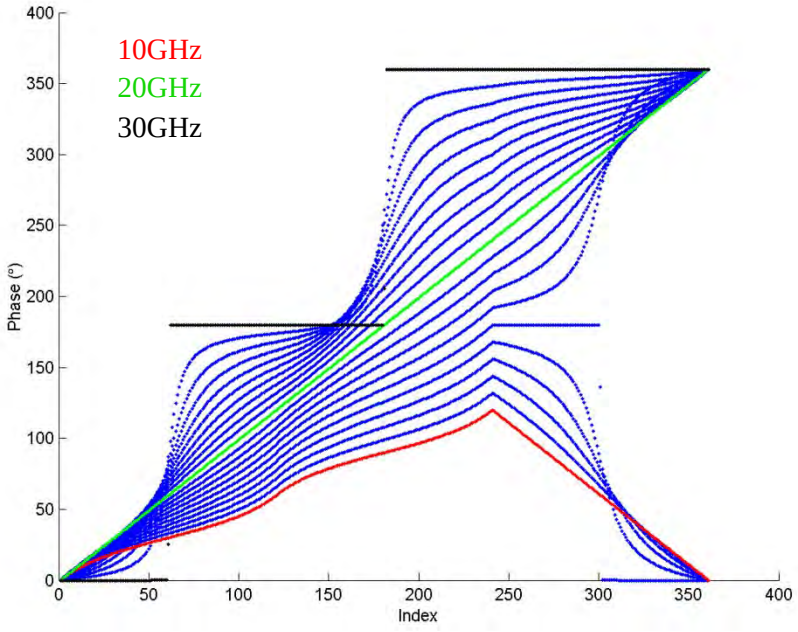

Figure 10: Phase vs. Index for 10GHz to 30GHz in 1GHz steps.

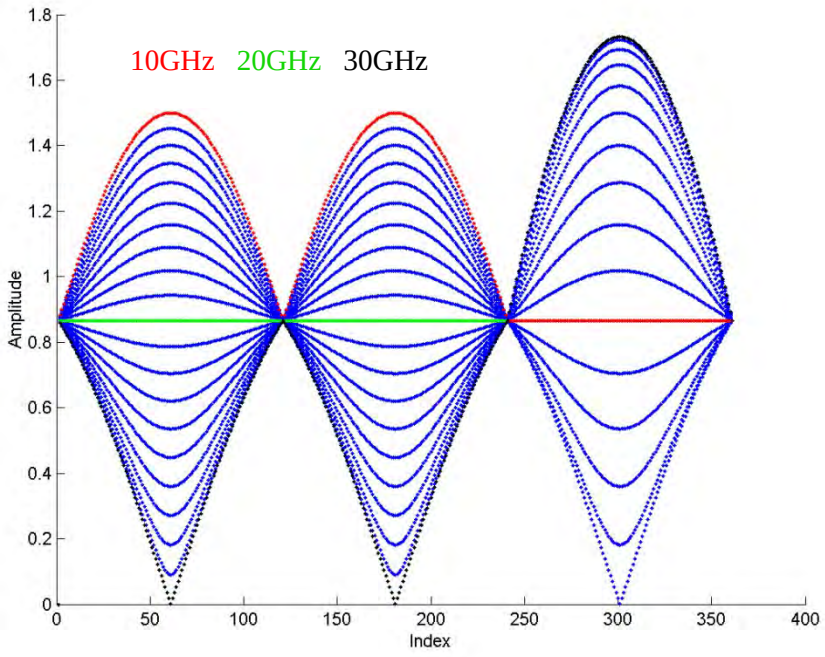

Figure 11: Amplitude vs. Index for 10GHz to 30GHz in 1GHz steps.

Next we can explore the bandwidth limitations. Figures 10 and 11 plot the phase and amplitude respectively from 10GHz to 30GHz in 1GHz, where 10GHz, 20GHz and 30GHz are color coded. The amount of phase shift possible is decreased to 180˚ by 15GHz, at which point the amplitude penalty is a 41% change (when looking at the indices range 0-240). At frequencies lower than 15GHz the phase shift possible in conjunction with the change in amplitude render the system un-useful. As frequency is increased the phase values obtainable decrease until at 30GHz only 0˚, 180˚, and 360˚ are possible. At 25GHz the amplitude also experiences a 48.2% change (~3dB) in the indices range of 0-240. At higher indices (240-360) the amplitude efficiency severely decreases as there is a 100% change possible at 15GHz and 73.2% change at 25GHz.

Lastly, we'll look at a 10% bandwidth, where almost 360˚ phase is achievable from 18GHz to 22GHz. The phase and amplitude are plotted from 18GHz to 22GHz in 0.5GHz steps in Figures 12 and 13 respectively. The amplitude at 18GHz and 22GHz has a 37.2% and 33.8% change possible over all indices respectively, which indicates that the phase to amplitude efficiency is worse as you decrease frequency from the 20GHz set center frequency. Earlier for Figure 11, the amplitude penalty appears to be higher for 25GHz when compared to 15GHz, but this is only because we were looking at the usable range of indices (0-240) and removing the higher ones which had a more severe amplitude penalty for the 15GHz case. For a smaller bandwidth window we would like to use all the indices and thus in this case the higher frequency shows a lower amplitude penalty.

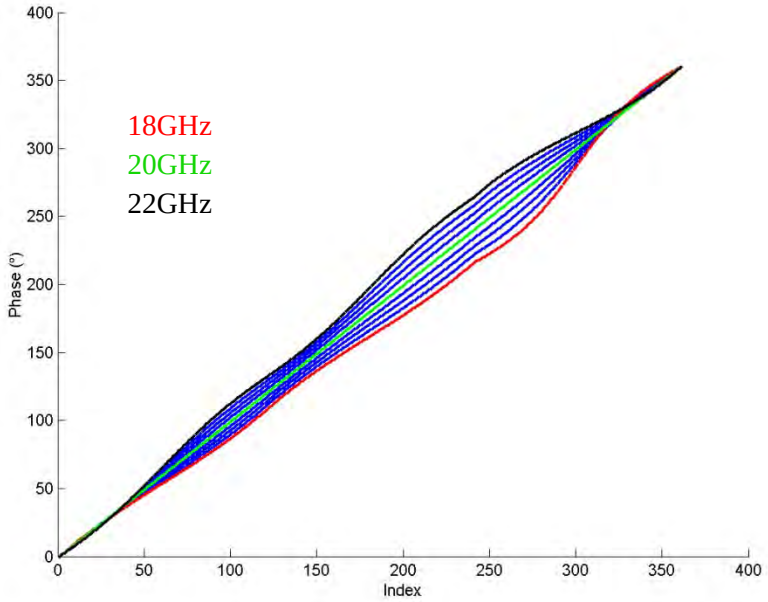

Figure 12: Phase vs. Index for 18GHz to 22GHz in 0.5GHz steps.

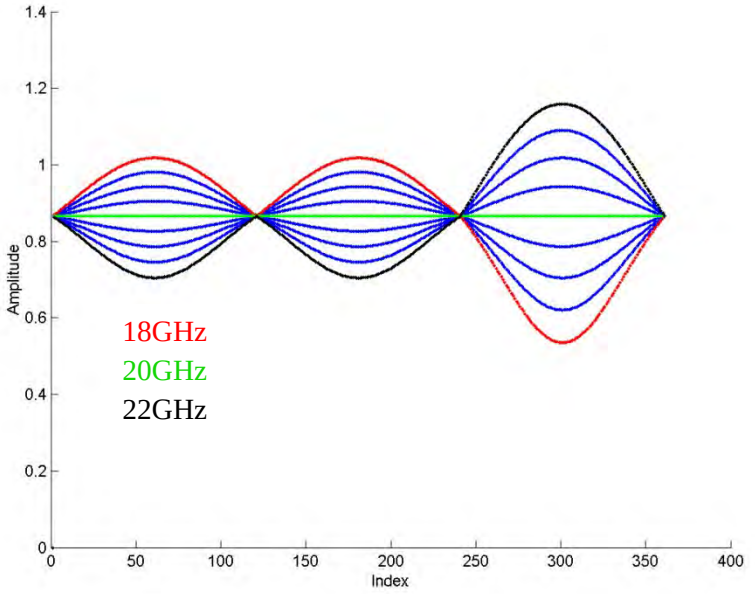

Figure 13: Amplitude vs. Index for 18GHz to 22GHz in 0.5GHz steps.

Another aspect that is useful to analyze is the comparison to a true time delay system. If a single phase is selected for the 20GHz phase, the error can be plotted as a function of frequency. The phase error as a function of frequency is plotted in Figure 14 for 30˚, 90˚ and 180˚. That is, the phase response of this architecture is compared to a single TTD that produces a 30˚, 90˚ or 180˚ phase shift at 20GHz. At 180º

there is no phase error from 0-30GHz. Both 30º and 90º have less than 5˚ phase error up to 20GHz, but the error increases rapidly up to 45˚ at 30GHz.

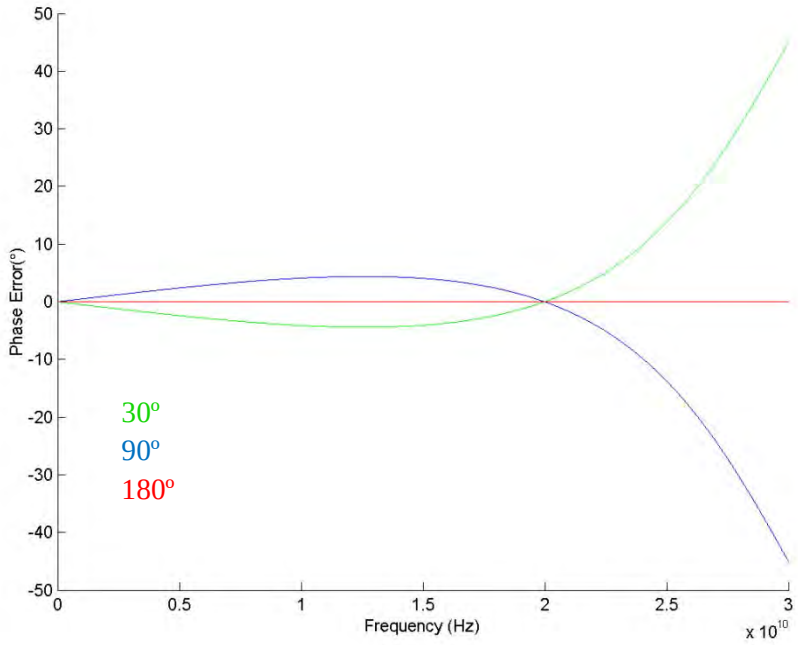

Figure 14: Error in phase from true time delay vs. frequency with center frequency 20GHz for 30º, 90º, and 180º.

In order to demonstrate the concept through measurement a 1x3 coupler setup was assembled using a DFB laser at wavelength 1550nm and three DSC30 photodiodes (PDs). Additionally, after two of the PDs, an electrical delay controller was inserted to fine tune the time delay lengths which were tuned to 20GHz. Measurements were made by changing the amplitudes with variable optical attenuators and measuring both phase and amplitude as a function of frequency from 0-20GHz. Since phase matching to 20GHz is very sensitive and the delay lengths can change due to minor temperature fluctuations, data is only presented up to 15GHz at which point the phase angles achieved are stable to within about ±2˚. Data was taken at different combinations of amplitudes to show the range of phase shift achievable at 15GHz, which should be 180˚ according to the analysis in Figure 5. In Figure 15, the phase is plotted as a function of frequency from -4˚ to 167˚ at 15GHz, which was the maximum range we were able to achieve or 95% of the theoretical range shown in Figure 5. In Figure 16 the corresponding amplitude as a function of frequency is plotted up to 15GHz, where we see that in general the larger the phase desired the larger the total amplitude fluctuation, where for a phase of -4˚ the amplitude is about 15dB lower than for 13˚, making that somewhat impractical to operate at since very little power is achievable at that phase angle.

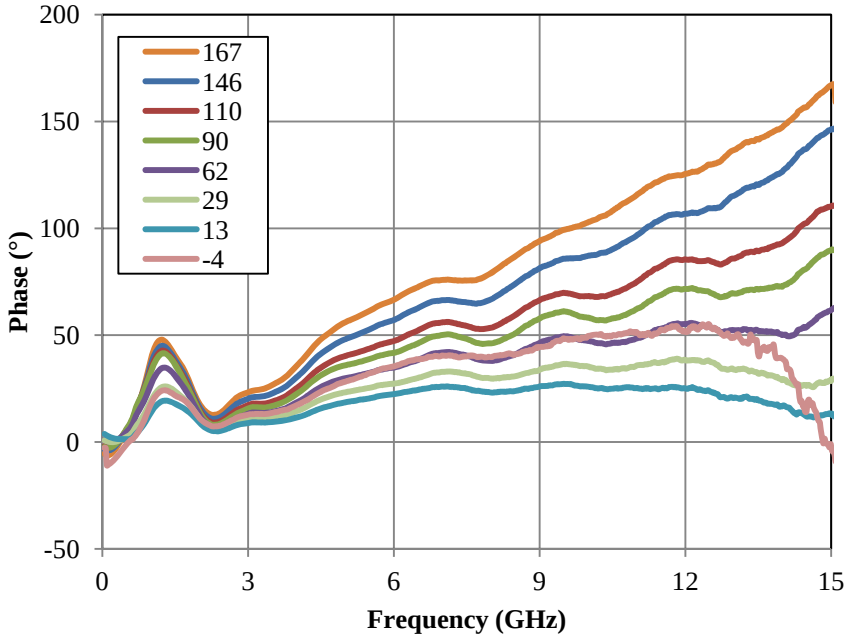

Figure 15: Measured phase vs. frequency for 1x3 coupler.

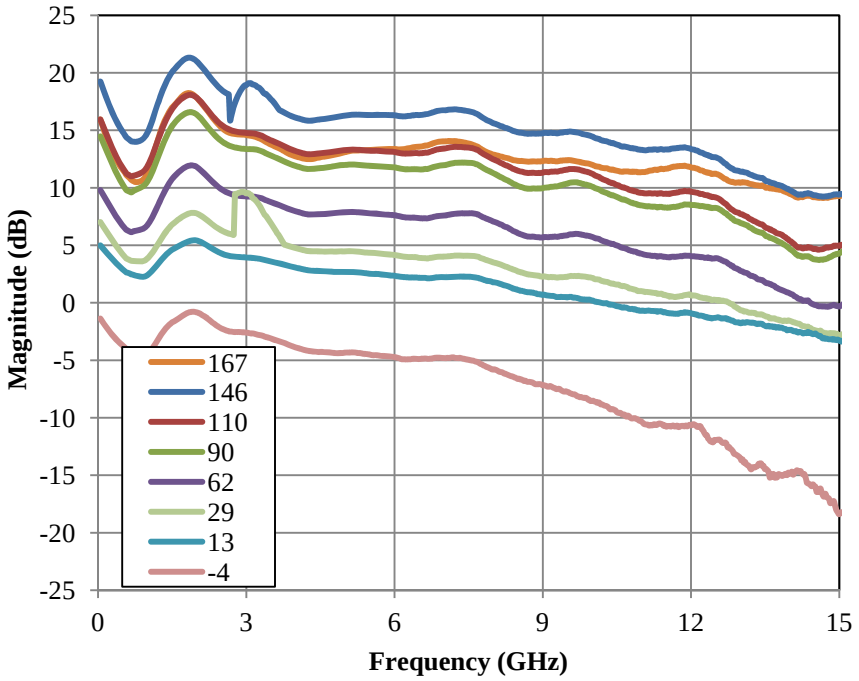

Figure 16: Corresponding measured amplitude vs. frequency for 1x3 coupler from Figure 19.

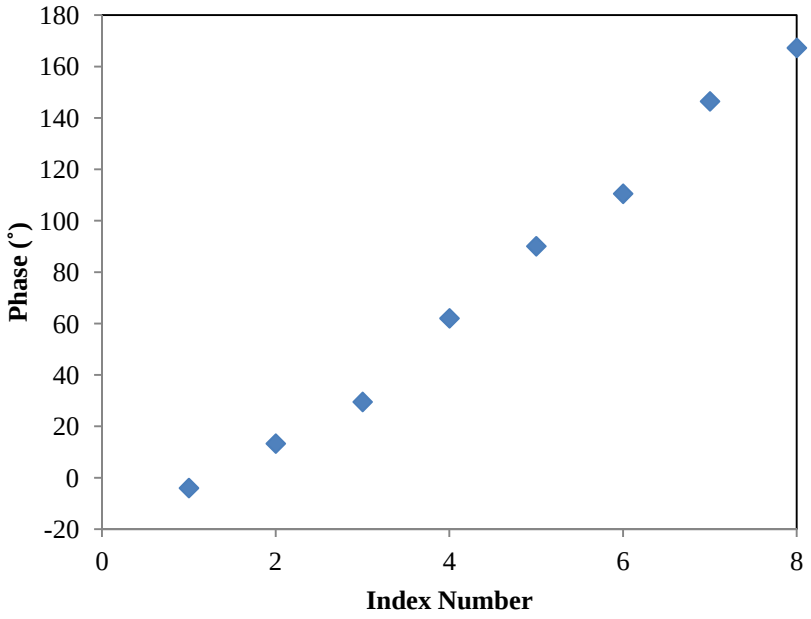

Figure 17: Measured phase as a function of index at 15GHz from Figure 19.

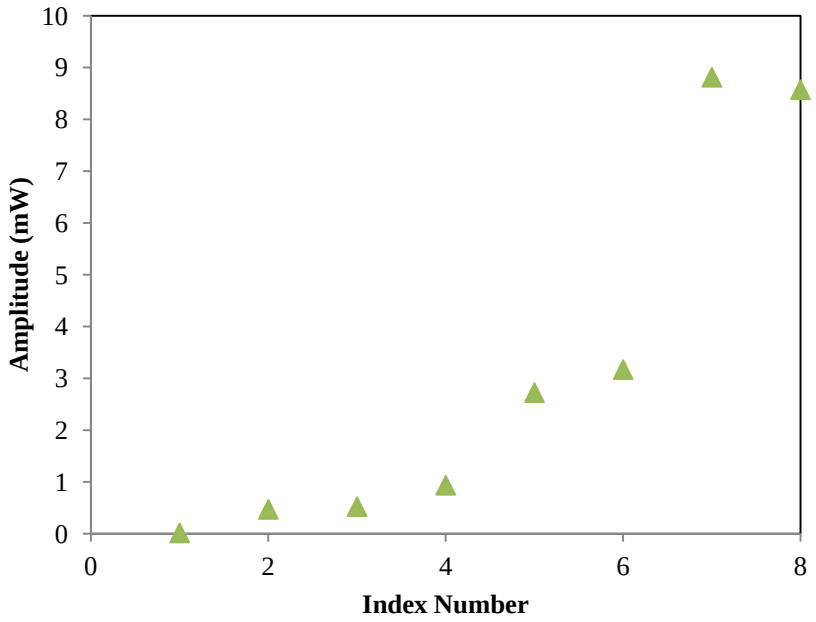

Figure 18: Measured amplitude as a function of index at 15GHz from Figure 20.

We will also plot phase as a function of index for the measured data taken in order of increasing phase and the corresponding amplitudes at 15GHz in Figures 17 and 18 respectively. In Figure 17, we can obtain a large range of phase shift (here only 8 points are shown as example). The amplitude is plotted in mW to show the phase to amplitude conversion. In the measurement system the amplitudes selected were

not based on the calculations completed for constant amplitude, where we would only use 2 of the 3 arms at any given time.

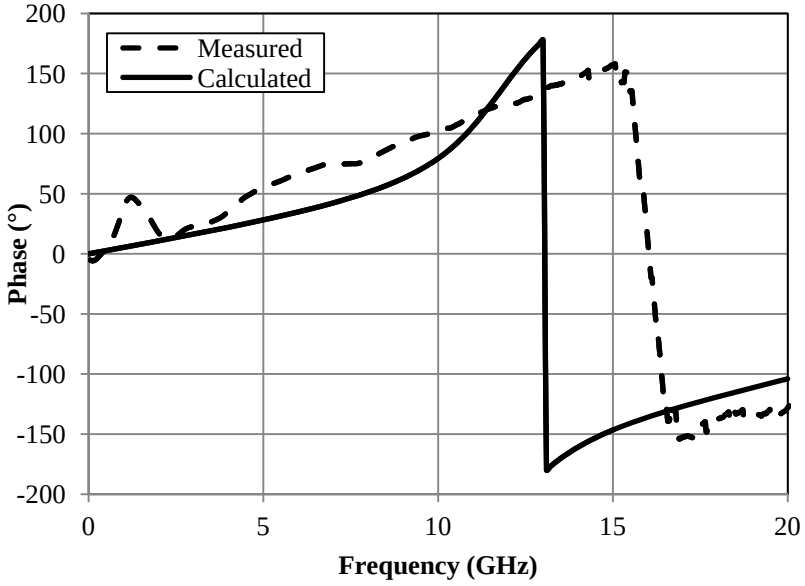

Figure 19: Phase as a function of frequency for measured and calculated with A_1=.929, A_2=.929 and A_3=2.33.

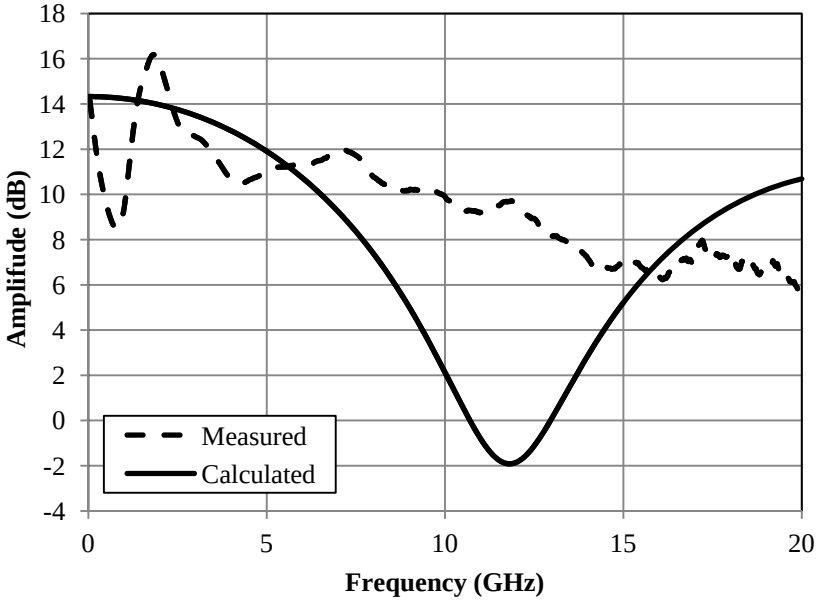

Figure 20: Amplitude as a function of frequency for measured and calculated with A_1=.929, A_2=.929 and A_3=2.33.

Finally, the measured and calculated phase and amplitude are plotted against each other as a function of frequency for the specific case at a measured phase of 157˚ at 15GHz in Figures 19 and 20 respectively. In this case, we recorded the attenuation amounts and the original power with no attenuation

to back out the amplitude coefficients of A_1=.929mW, A_2=.929mW and A_3=2.33mW in order to calculate the theoretical plots. There is good agreement with the phase except that the peak occurs at a slightly higher frequency that the calculated data. Possible reasons for this include the accuracy of our phase matching as well as the accuracy in the calculation of the coefficients. In Figure 20, the measurement data does not show the large dip near 12GHz that is predicted in the calculated data. Since the calculation was somewhat off in Figure 19, it is reasonable to assume that our amplitude shape will also not be accurate in the calculation. Further study with more precise measurement of the coefficients and phase matching will help to reconcile our theory and measurement data.

4. Summary and Conclusion

In conclusion, we have demonstrated mathematically a phase shifter employing time delay, for 1x3 coupler. Additionally, simulations provided insight in the bandwidth and limitations of each system. We solved mathematically for constant amplitude with 360º phase shift and showed a 10% usable bandwidth with less than 3dB amplitude penalty from 18GHz to 22GHz. Finally, the system was built and tuned to 20GHz center frequency. Results for phase and amplitude range as a function of frequency showed good agreement with the theoretical simulations. Additionally, phase and amplitude as a function of index was plotted to show that 180˚ phase shift is possible at 15GHz frequency as predicted by the simulations. The photonic phase shifting method described here has potential use in PAA systems, where the scalability and bandwidth afforded by fiber optics can be utilized. However, the complexity of this particular technique in such an architecture must be considered. Every element that requires phase shifting would require three variable optical attenuators, three photodiodes and a device to combine the three photocurrents.

References

[1] R. J. Mailloux, *Phased Array Antenna Handbook* (Artech, 1994).

[2] W. Li, N. H. Ahu and L. X. Wang, "Photonic phase shifter based on wavelength dependence of Brillouin frequency shift," IEEE Photon. Technol. Lett., vol. 23, no. 14, pp. 1013-1015, Jul. 15, 2011.

[3] I. Frigyes and A. J. Seeds, "Opticall generated true-time delay in phased-array antennas," IEEE Trans. on Microw. Theory and Tech., vol. 43, no. 9, pp. 2378-2386, Sept. 1995.

[4] H. Zmuda and E. N. Toughlian, Photonic Aspects of Modern Radar. Norwood, MA: Artech house, 1994.

[5] W. S. Birkmayer and M. J. Wale, "Proof-ofconcept model of a coherent optical beam-forming network," IEE Proceed. J. Optoelectronics, vol. 139, no. 4, pp. 301-304, Aug. 1992.

[6] D. B. Adams and C. K. Madsen, "A novel broadband photonic RF phase shifter," J. Lightw. Technol., vol. 26, no. 15, pp. 2712–2717, Aug. 1, 2008.

[7] R. T. Schermer, F. Bucholtz, and C. A. Willarruel, "Continuously-tunable microwave photonic true-time-delay based on fiber-coupled beam deflector and diffraction grating," Optics Express, vol. 19, no. 6, March 14, 2011.

Appendix A: Theory for 1x4 Coupler (M=4)

For the 1×4 coupler case, the photocurrent is determined by (1) where $\tau_1 = 0$, $\tau_2 = 1/8f_0$, $\tau_3 = 1/4f_0$ and $\tau_4 = 3/8f_0$ for each receiver output respectively. Figure A.1 plots the combined photocurrent vs. time at $f_0 = 20$GHz and $f = 20$GHz with amplitudes varied from 0 to 1 with a 0.5 step size. At 20GHz, similar to the 1×3 coupler case there is a large amount of phase shift possible. This is further evidenced by Figure A.2, which shows the phase vs. frequency with amplitudes varied the same as in Figure A.1. In this instance the 0 or 180 degree phase shift occurs at $f = (4k - 2)f_0$ while the 0 or 360 degree shift occurs at $f = (4k)f_0$ where k=1, 2, 3, … As in Figure 11, Figure A.3 shows a zoomed in view of Figure A.2 with a single case highlighted in red to show the shape of the phase shift versus frequency.

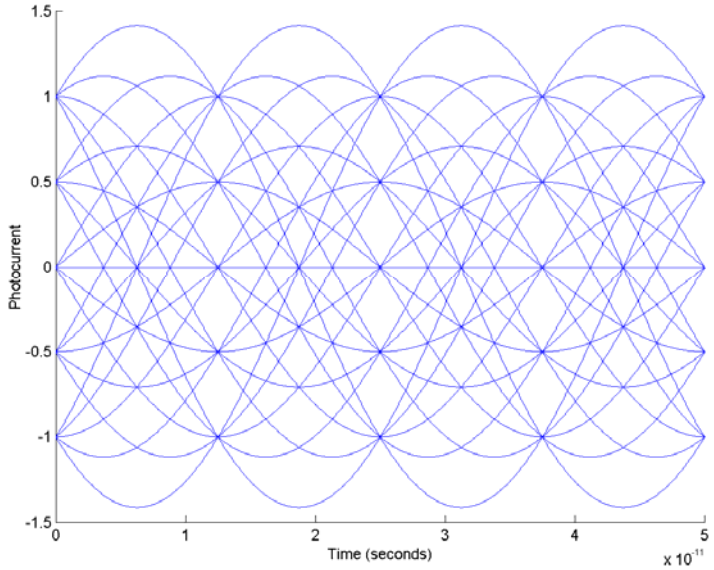

Figure A.1: Photocurrent vs. time for 1×4 coupler at 20GHz with amplitudes varied from 0 to 1.

As with the 1x3 coupler case, the 1x4 coupler was evaluated for a specific set of coefficients over a bandwidth of 100GHz. In Figure A.4 the phase and amplitude are plotted for A_1=0.23, A_2=0.45,

A_3=0.87, and A_4=0.90. There are both major and minor peaks and nulls, with minor nulls at multiples of 40GHz and major peaks at multiples of 80GHz. The derivative of phase (blue) is plotted with amplitude in Figure A.5 to illustrate that the nulls occur where the first derivative of phase has an inflection point which is the same as in the 1x3 coupler case.

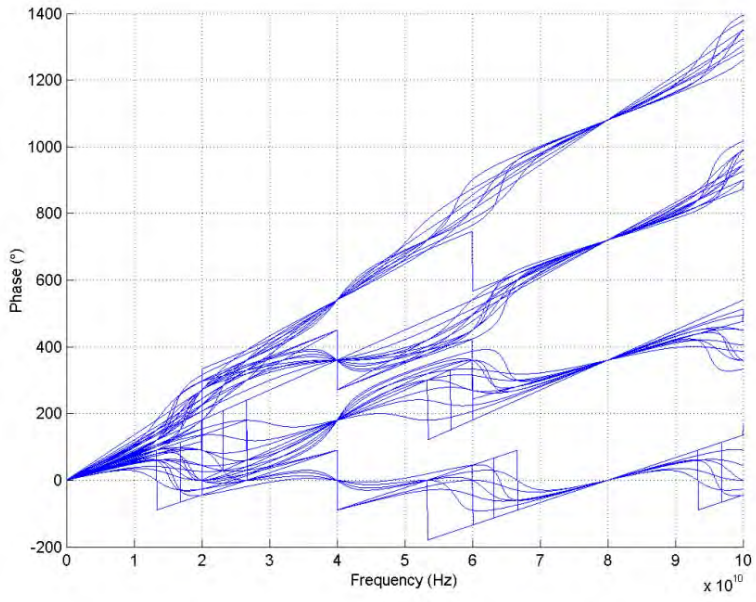

Figure A.2: Phase vs. frequency for 1×4 coupler with amplitudes varied from 0 to 1 with 0.5 steps.

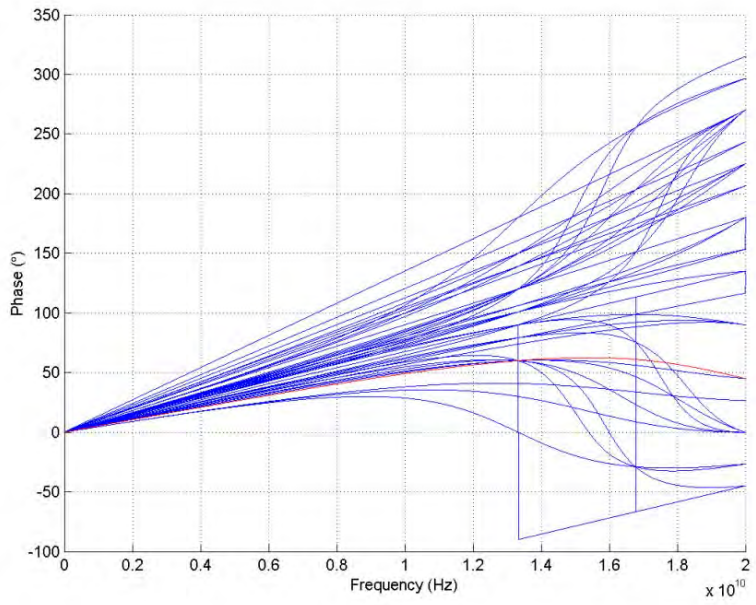

Figure A.3: Zoomed in view of Figure 13 from 0-20GHz.

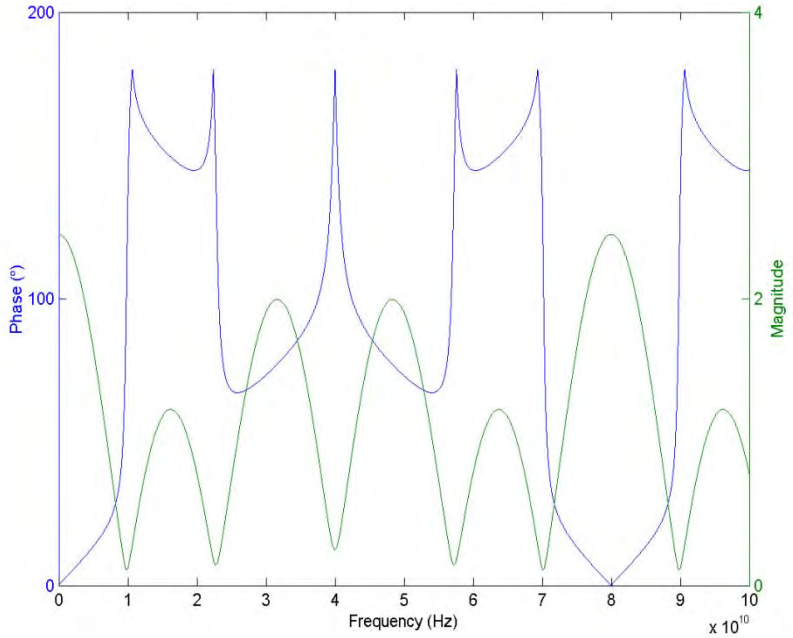

Figure A.4: Phase (blue) and amplitude (green)vs. frequency for A_1=0.23, A_2=0.45, A_3=0.87, and A_4=0.90.

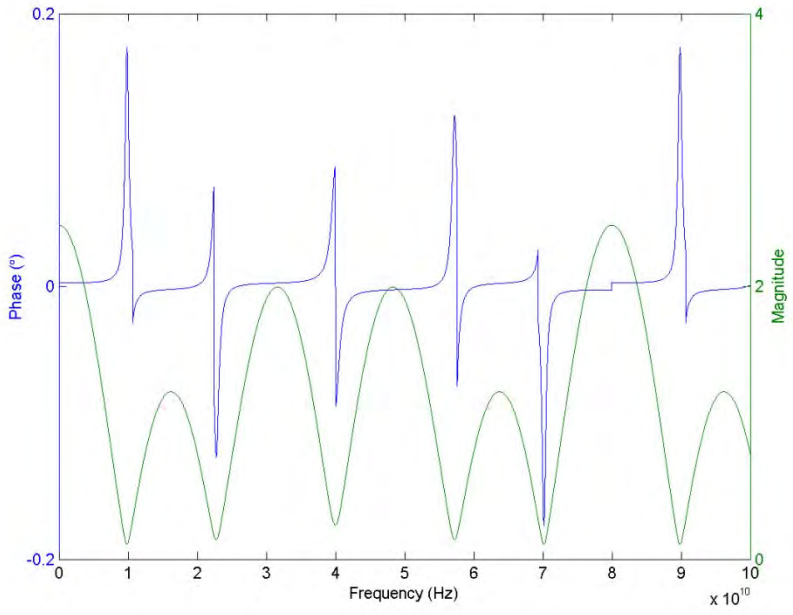

Figure A.5: Derivative of phase (blue) and amplitude (green) vs. frequency for coefficients A_1=0.23, A_2=0.45, A_3=0.87, and A_4=0.90.

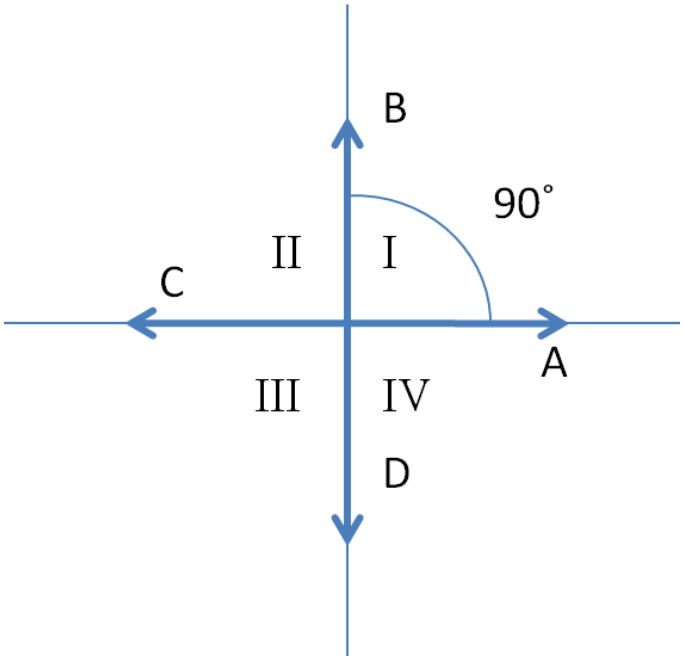

Figure A.6: Diagram of each vector used to solve for constant amplitude for 1x4 coupler.

As we previously laid out the steps for finding solutions for constant amplitude in Section 3, we can solve similar equations for the case of a 4x1 coupler. In this case there are four vectors that occur on each axis. The amplitude we will solve for is 1. The general equations we have for the circle are:

$$1 = \sqrt{(A-C)^2 + (B-D)^2} \qquad (A.1)$$

$$\theta = tan^{-1}\left(\frac{B-D}{A-C}\right) \qquad (A.2)$$

With two equations and four unknowns we can solve the equations in 4 parts. In each case we zero two vectors and solve in quadrant I, II, III and IV as shown in Figure A.6. In order to compare to the 3x1 coupler case, we repeat the same calculations starting with phase and amplitude from 10GHz to 30GHz in 1GHz steps which is plotted in Figures A.7 and A.8 respectively. In comparison to the 1x3 coupler case there is not a huge benefit to the phase but the amplitude has a smaller penalty.

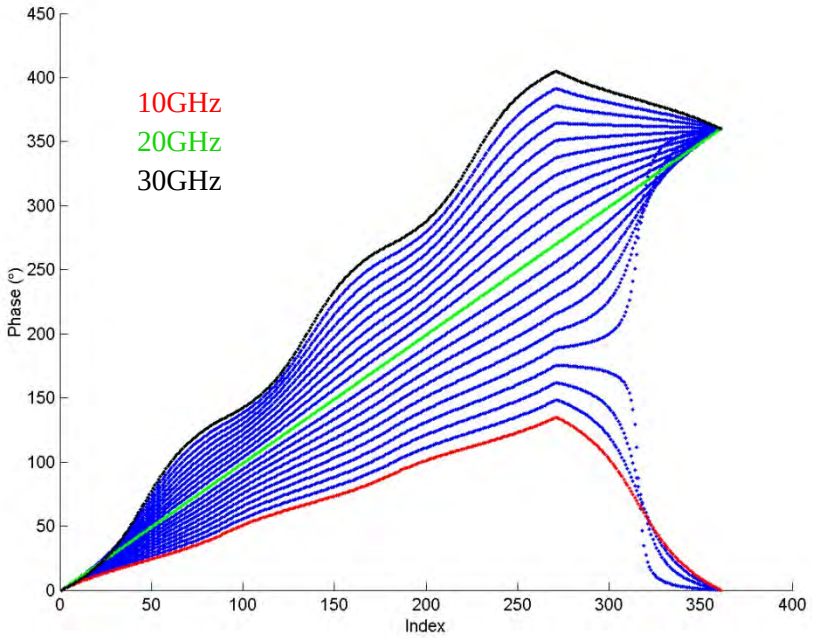

Figure A.7: Phase vs. Index for 10GHz to 30GHz in 1GHz steps for 1x4 coupler.

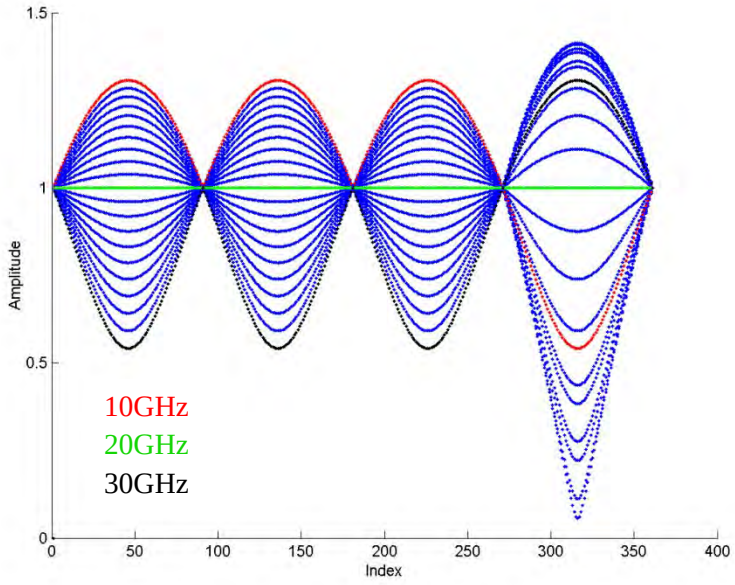

Figure A.8: Amplitude vs. Index for 10GHz to 30GHz in 1GHz steps for 1x4 coupler.

As in section 3, we will look at a 10% bandwidth which is plotted from 18GHz to 22GHz in 0.5GHz steps for phase and amplitude in Figures A.9 and A.10 respectively. In this case the maximum

amplitude penalty is 20.5% at 22GHz and 26.1% at 18GHz which is slightly less than for the 1x3 coupler case.

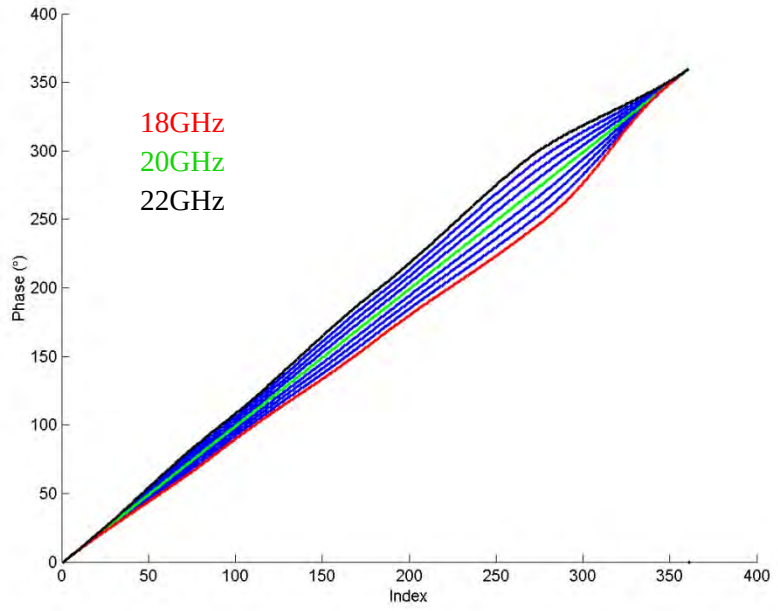

Figure A.9: Phase vs. Index for 18GHz to 22GHz in 0.5GHz steps for 1x4 coupler.

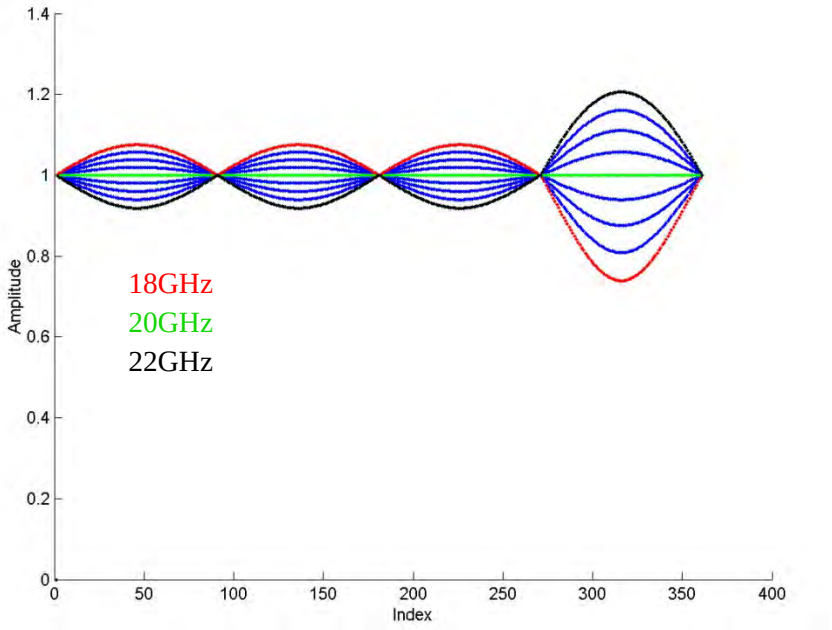

Figure A.10: Amplitude vs. Index for 18GHz to 22GHz in 0.5GHz steps for 1x4 coupler.

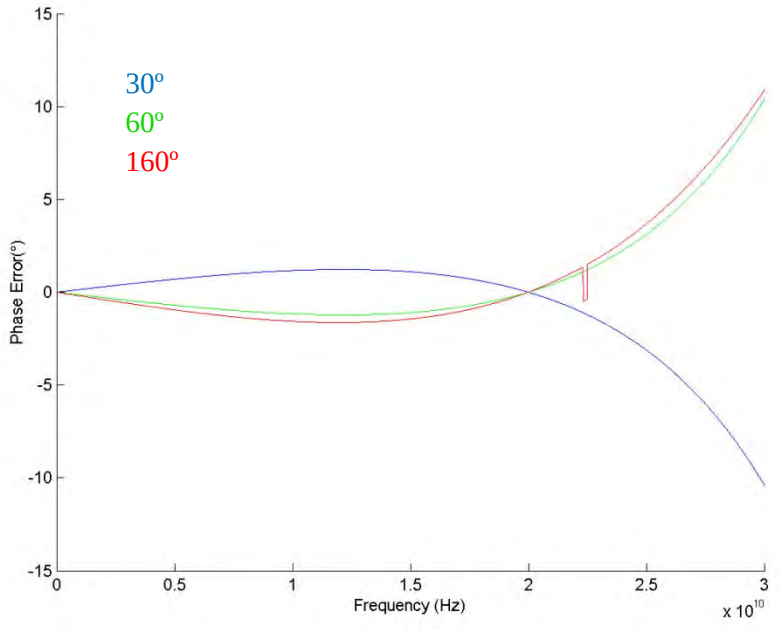

Figure A.11: Error in phase from true time delay vs. frequency with center frequency 20GHz for 30º, 60º, and 160º for 1x4 coupler.

Finally, we will look at the error in phase when compared to TTD as a function of frequency which is plotted in Figure A.11 for 30˚, 60˚, and 160˚. The phase error is less than 2˚ up to 20GHz for both 30˚ and 60˚. For the 30˚ case the phase error increases to 12˚ at 30GHz, which is less than the 45˚ phase error resultant for 30˚ in the 1x3 coupler case, demonstrating that the increased complexity of using a 1x4 coupler design will result in a smaller amount of phase error when compared to TTD than the 1x3 coupler setup.

Appendix B: Theory for 1xM Coupler

Finally, certain general rules can be established for the case of a 1×M coupler. The photocurrent will be generalized as:

$$I_n = A_n \sin(2\pi f(t + \tau_n)) \tag{B.1}$$

where $\tau_n = 2\pi n/M\omega_0$ for n= 1, 2, …M. Additionally, there will be frequencies where only 0 and 180 degree phase shift occurs:

$$f = \left(Mk + \frac{M}{2}\right) f_0 \tag{B.2}$$

where k=1,2,3,… Finally, no phase shift will occur at certain frequencies defined by:

$$f = (Mk) f_0 \tag{B.3}$$

From the three cases that were studied, it is obvious that as M increases the lowest frequency at which (B.2) and (B.3) apply increases as well as the precision and amount of phase shift that is achievable at lower frequencies, with the trade off of a more complicated architecture.

Additionally, certain behaviors for the amplitude and phase as a function of frequency can be defined. From Figure 12, the null in the amplitude to occur at:

$$I_{null} = \frac{f_0 M}{2} k \qquad (B.4)$$

where k=1, 2, 3... The major peaks in amplitude will then occur at:

$$I_{peak} = f_0 M k \qquad (B.5)$$

where k=0, 1, 2, 3...